LETTERS

Continental ice in Greenland during the Eocene and Oligocene

James S. Eldrett[1]†, Ian C. Harding[1], Paul A. Wilson[1], Emily Butler[1] & Andrew P. Roberts[1]

The Eocene and Oligocene epochs (~55 to 23 million years ago) comprise a critical phase in Earth history. An array of geological records[1–5] supported by climate modelling[6] indicates a profound shift in global climate during this interval, from a state that was largely free of polar ice caps to one in which ice sheets on Antarctica approached their modern size. However, the early glaciation history of the Northern Hemisphere is a subject of controversy[3,7–9]. Here we report stratigraphically extensive ice-rafted debris, including macroscopic dropstones, in late Eocene to early Oligocene sediments from the Norwegian–Greenland Sea that were deposited between about 38 and 30 million years ago. Our data indicate sediment rafting by glacial ice, rather than sea ice, and point to East Greenland as the likely source. Records of this type from one site alone cannot be used to determine the extent of ice involved. However, our data suggest the existence of (at least) isolated glaciers on Greenland about 20 million years earlier than previously documented[10], at a time when temperatures and atmospheric carbon dioxide concentrations were substantially higher.

The existence of Northern Hemisphere ice sheets can be demonstrated back to the middle Miocene (~15 million years ago), on the basis of proxy data and direct documentation of ice-rafted debris (IRD) from the Nordic seas[9–11]. There are few records of earlier Cenozoic glacial activity in the boreal realm because most marine sedimentary sections of this age suffer from extremely poor age control, slow sedimentation rates and widespread hiatuses. These problems are widely assumed to have resulted from increased ocean circulation strength and glacioeustatic sea-level fall associated with ice build-up on Antarctica[12]. Therefore, failure to document IRD from pre-mid-Miocene sediments in the Northern Hemisphere should not be interpreted to indicate that ice was restricted to Antarctica alone. To understand better Eocene-Oligocene palaeoceanographic and palaeoclimatic events in the high northern latitudes we have generated a new stratigraphy for three key Deep Sea Drilling Project (DSDP)/Ocean Drilling Program sites (ODP sites 338, 643 and 913; Fig. 1a) by calibrating dinocyst events to the geomagnetic polarity timescale[13]. The most complete Eocene to Oligocene succession is provided by ODP site 913 (75° 29.356' N, 6° 56.810' E, present

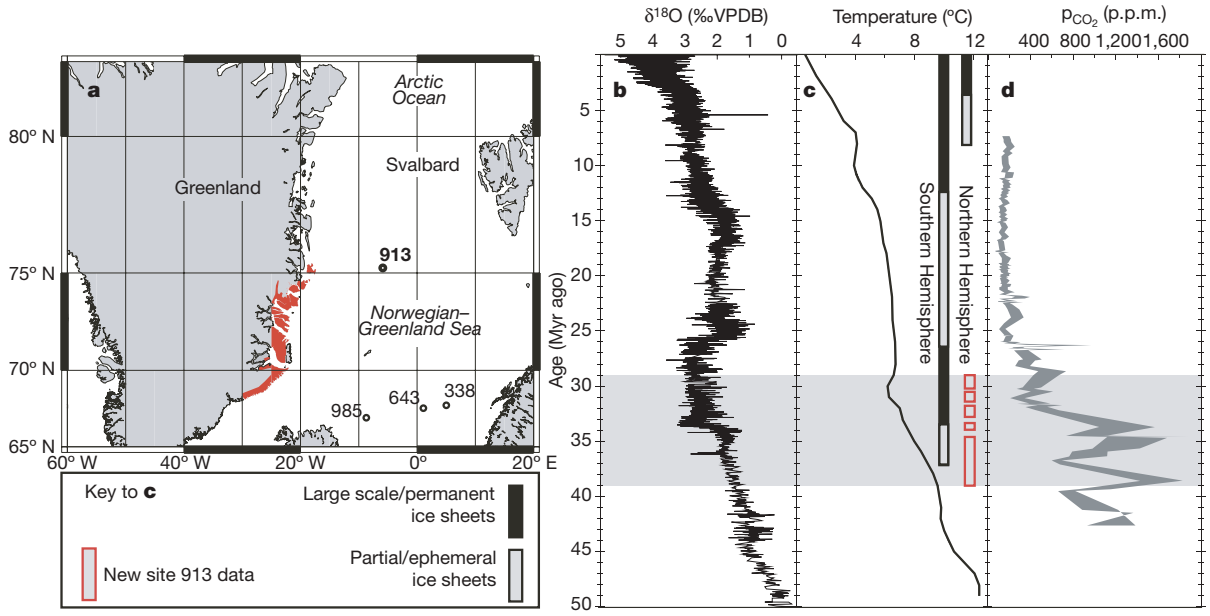

Figure 1 | Eocene–Oligocene palaeoclimate records and location of site 913. a, The location of site 913 (ODP Leg 151) and other sites referred to in the text. The area of East Greenland shaded in red indicates our inferred source area for the IRD: the Cretaceous–Cenozoic sedimentary basins and Palaeogene igneous outcrops from Kangerlussuaq in the south to Shannon Island in the north. **b**–**d**, The grey box indicates the stratigraphic interval studied here set against the benthic $\delta^{18}O$ curve from ref. 1 (**b**) and the Mg/Ca-based bottom water temperatures from ref. 2 (**c**), against which are set in black/grey the generally accepted chronology of southern and Northern Hemisphere Cenozoic glaciation as presented in ref. 1, and the view based on our data in red. VPDB, Vienna Pee-Dee belemnite standard. **d**, The CO_2 partial pressure curve from ref. 29.

[1]School of Ocean and Earth Science, National Oceanography Centre Southampton, University of Southampton, European Way, Southampton SO14 3ZH, UK. †Present address: Shell UK Ltd, 1 Altens Farm Road, Nigg, Aberdeen AB12 3FY, UK.

water depth ~3,300 m). All magnetic polarity chrons from chron C18n.2n to chron C11n are present with the exception of chron C13n, which we interpret to fall in the core gap that spans the Eocene–Oligocene boundary (Fig. 2a).

The Eocene–Oligocene section from ODP site 913 is carbonate-free, and is primarily composed of laminated biosiliceous ooze, overlain by clays and biosiliceous clays (Fig. 2b)[14]. Laminations are particularly pronounced from 471.6 m below sea floor (m.b.s.f.) to ~500 m.b.s.f. Initial shipboard investigations identified an isolated, macroscopic lithic clast at 453.16 m.b.s.f. but concluded that it was the result of down-hole contamination from the overlying Miocene glacial sequence, rather than an *in situ* glacially derived clast[14]. To test this shipboard interpretation, we undertook an investigation of the Eocene–Oligocene sequence at ODP site 913B. Our detailed core observations reveal the presence of *in situ* macroscopic clasts (up to 3.5 cm in length) from cores 27R to 21R (from the top of chron C18n.1n through to chron C17n.2-3n, and within chrons C15r, C12r and C11r: that is from ~38 to 30 Myr ago; Fig. 2a, b), which argue against the shipboard interpretation of drilling contamination. To determine the origin of these clasts, we undertook a microscopic examination of their surface features and made detailed observations of the cores in which they occur. We interpret the impact-induced deformation of laminae underlying clasts at 494.32 m.b.s.f. and 492.76 m.b.s.f. (C17n.3n, Fig. 3a, b) in this otherwise fine-grained pelagic sedimentary succession to be indicative of a dropstone origin. A 3.5-cm-long unfoliated gneissic clast at 492.9 m.b.s.f. (C17n.3n, Fig. 3c, d) reveals a prominent gouge with well-developed parallel striations. Other clasts display surficial microscopic conchoidal fractures (for example, a 3-cm-long vein quartz clast at 453.29 m.b.s.f.; C12r). These surface features are all consistent with glacial abrasion and crushing, and support an ice-rafted origin for these dropstones. Although glacially derived sediments deposited at the shelf edge by advancing continental glaciers could have been transported downslope by gravity flow, our dropstone-bearing interval lacks sedimentary structures indicative of gravity flow-induced deposition (for example, debrites, graded bedding, Bouma sequences, and so on). Organic-carbon-rich laminated sediments, characteristic of anoxia at the sediment–water interface, are stratigraphically extensive in the studied material, and on the basis of all textural and sedimentary structure lines of evidence we rule out a mass flow transport mechanism for our dropstones.

To determine whether the dropstones are indicative of isolated or more pervasive ice-rafting, we analysed surface textures of microscopic grains, calculated mass accumulation rates (MARs) of different grain size fractions (>63, >125 and >250 μm), and determined the magnetic properties and whole-rock trace element geochemistry of the dropstone-bearing strata. Grain size samples were taken from 429.57 to 503.22 m.b.s.f., but sampling was not continued below core 28R owing to core disturbance and evidence of gravity flow deposits (for example, graded beds, sharp basal contacts, and so on). Scanning electron microscope analysis of >250 μm quartz grains from the interval yielding macroscopic dropstones indicates a high frequency of angular and high-relief grains, and surface morphological features (for example, striations, straight/arcuate steps and conchoidal fractures) that are diagnostic of mechanical breakage and sculpting of grain surfaces in glacial environments[5,11,15] (see Fig. 3e–l). These observations point towards pervasive ice rafting. Grain size fraction data can be used to help determine the mode of ice rafting. Analysis of surface sediment samples from the Arctic Ocean indicates that the >63 μm fraction is a minor component (≤1 wt%) of sediments rafted beyond the inner coastal zone by sea ice, but is a major constituent of sediments rafted by icebergs[16,17]. When downslope processes can be excluded, the presence of this grain size fraction has been taken as evidence for iceberg rafting[17–19]. On this basis, in the Eocene–Oligocene interval we studied, iceberg rafting appears to have played a much more important role than sea ice rafting (in ~90% of our samples the >63 μm size fraction formed >1 wt%; in ~75% of our samples it formed >5 wt%; and in ~10% of our samples it formed >30 wt%).

To provide comprehensive records of detrital mineral concentrations and to check whether there is a correspondence with IRD concentrations[20], we determined the mass magnetic susceptibility (χ) and the natural remanent magnetization (NRM) of the studied sediments. The magnetic properties of the sediments in the analysed

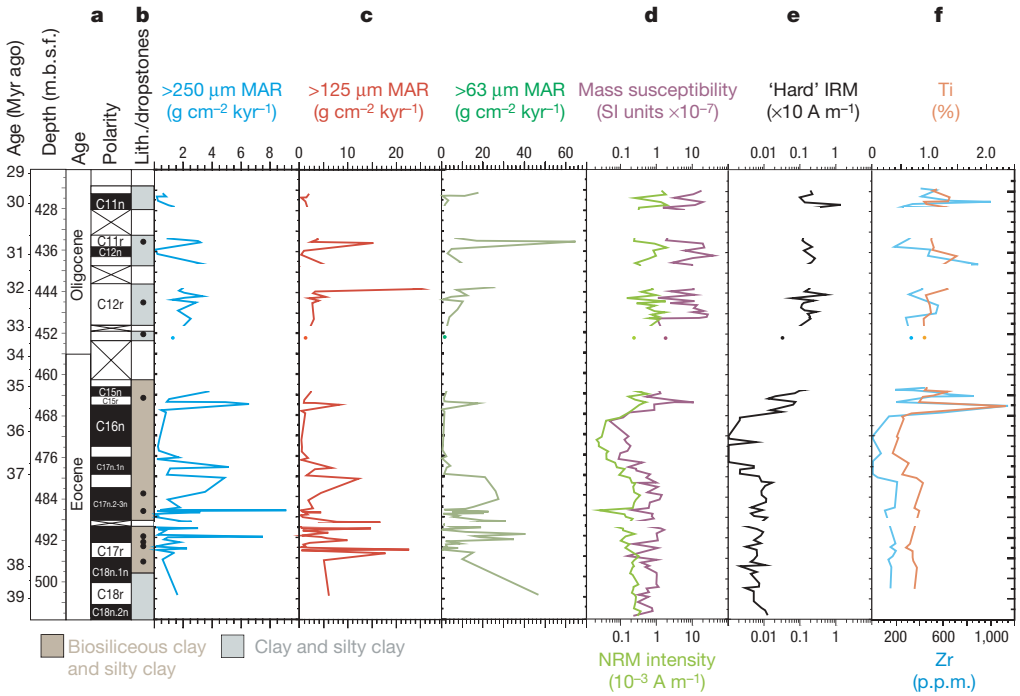

Figure 2 | Data from ODP site 913, Greenland Basin. **a**, Age model: the chronology for ODP site 913 is based on direct correlation to the geomagnetic polarity timescale reported in ref. 13. **b**, Lithology (Lith.) of the core, and positions of macroscopic dropstones (solid circles). **c**, Ice-rafted debris mass accumulation rate (MAR) of the >250, >125 and >63 μm grain size fractions. **d**, **e**, Magnetic parameters are mass susceptibility (χ), NRM and 'hard' IRM, respectively (note the logarithmic scales). **f**, Trace-element abundances of zirconium and titanium (see Methods).

section vary considerably with depth (Fig. 2d, e). The magnetic mineral concentration is lowest in the interval with the highest biogenic component (C16n). These low χ and NRM values most probably result either from dilution associated with increased flux of biogenic material, or from diagenetic dissolution of detrital magnetic minerals attributable to increased organic carbon content in the biosiliceous interval[21]. Above C16n, there is a step-shift to much higher magnetic mineral contents (where χ and NRM reach maximum values). Fine-grained magnetite is the dominant magnetic mineral responsible for the magnetic signal at ODP site 913[13]. However, increased values of the 'hard' isothermal remanent magnetization (IRM) suggest a significant additional contribution from high-coercivity magnetic minerals (principally haematite) above C16n. The step from a magnetite-dominated signal to a magnetite–haematite signal may demonstrate different source terrains feeding ODP site 913 in the Eocene versus the Oligocene. Our X-ray fluorescence geochemical data series from ODP site 913 also records a prominent up-section shift from lower to higher values of Zr and Ti towards the top of C16n (Fig. 2f). This shift indicates an increased heavy and/or detrital mineral content that is consistent with a contemporaneous increase in terrigenous component[22] (see Supplementary Information, Fig. 2f).

Our data also allow us to help constrain the provenance of the IRD found at ODP site 913 and thereby to shed light on the location of early Northern Hemisphere ice formation. The >63 μm fraction in our samples is dominated by quartz grains, but basic igneous, sedimentary and metamorphic lithic clasts are also found, and these are most common in samples from the interval containing the greatest number of macroscopic dropstones (~C18n.1n to C17r, ~38 Myr ago). The igneous clasts found throughout the Eocene sequence at ODP site 913, the haematite-dominated signal and the increase in titanium initiated within C16n (Fig. 2) are consistent with derivation from altered basalts. The provenance of this material may be the Palaeogene flood basalts of East Greenland, such as those on Hold with Hope[23] directly to the west of ODP site 913, but which have an extensive outcrop from Kangerlussuaq in the south to Shannon Island in the north (area marked in red in Fig. 1a). This hypothesis is supported by the presence of reworked early Eocene dinocysts above chron C16n at ODP site 913[13,24], which are compatible with those reported from the intra-basaltic Eocene sediments from East Greenland[25]. In addition, we have found dinocysts of late Cretaceous age[24], which are also known from sediments of Cenomanian to Maastrichtian age in East Greenland[26]. This observation is important because it allows us to rule out Svalbard as a potential source region, as post-Albian Cretaceous strata are absent from Svalbard[27].

Our data demonstrate that ice rafting to the Norwegian–Greenland Sea was active at least intermittently between 38 and 30 Myr ago at ODP site 913. Iceberg ice had an important role in delivering the IRD that we document, with East Greenland as the source (Fig. 1a). On the basis of our records alone, we cannot determine whether substantial ice-sheets existed on Greenland at this time, or whether the IRD originated from smaller, isolated glaciers. It remains to be seen, therefore, whether the events that we have documented would have significantly affected the isotopic composition of the contemporaneous ocean. Resolution of these questions has global implications because of the ongoing debate concerning Cenozoic ice budgets, the timing of the inception of Northern Hemisphere glaciation[2,3,7,9,12], and our

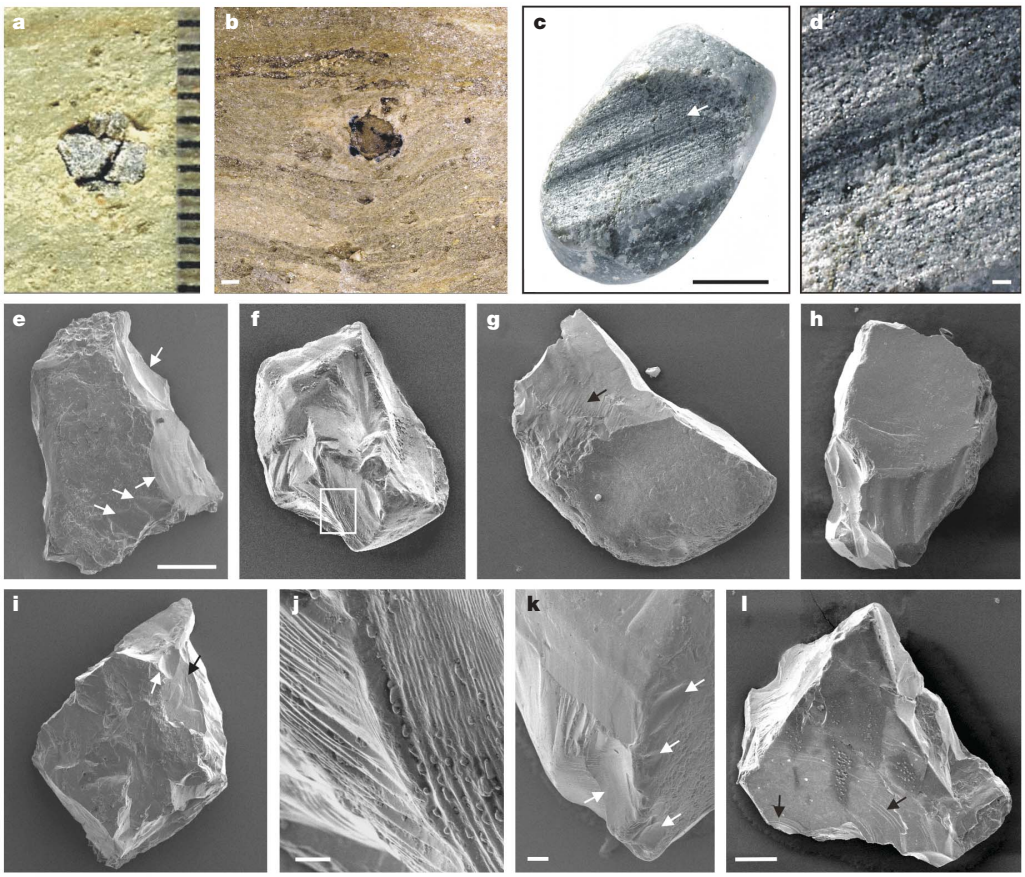

Figure 3 | Representative images of dropstones and quartz grains. **a**, **b**, *In situ* dropstones with impact-induced deformation of underlying laminae (**a**, 494.32 m.b.s.f.; **b**, 492.76 m.b.s.f.). **c**, **d**, Unfoliated gneissic dropstone from 492.9 m.b.s.f. with prominent gouge (white arrow in **c**) containing parallel striations. **d**, Detail of striations seen in **c**. **e**–**l**, Representative scanning electron microscope images of >250 μm quartz grains from 486.5 m.b.s.f., showing surface features indicative of glacial environments. White arrows in **e**, **i** and **k** indicate conchoidal fractures. Black arrows in **g**, **i** and **l** denote straight or arcuate stepped fractures, also shown in **f**. **j** is a magnified view of the area inside the white box in **f**. Scale bars: **a**, **b**, **d**, 1 mm (ruler scale in millimetres to the right of **a**); **c**, 1 cm; **e**–**i**, 100 μm (scale bar as in **e**); **j**, **k**, 10 μm; **l**, 100 μm.

understanding of Cenozoic atmospheric carbon dioxide levels (Fig. 1). Recent palaeoclimate model experiments generate substantial ice sheets in the Northern Hemisphere for the Eocene only in runs where carbon dioxide levels are lower (approaching the pre-anthropogenic level, $\sim 1 \times$ PAL) than suggested by proxy records (~ 7 to $2 \times$ PAL, Fig. 1d)[28,29]. Regardless, our data provide the first stratigraphically extensive evidence for the existence of continental ice in the Northern Hemisphere during the Palaeogene. This is about 20 Myr earlier than previously documented (mid-Miocene)[10], at a time when global deep water temperatures and, by extension, surface water temperatures at high latitude, were much warmer (Fig. 1c). By inference, our data strengthen the case for the existence of some ice in the Northern Hemisphere even earlier in the Cenozoic, as suggested by results from Integrated Ocean Drilling Program (IODP) site 302 (ref. 9), and for more extensive ice-sheets at the glacial maximum of the Eocene–Oligocene transition, as suggested by results from ODP site 1218 (ref. 3).

METHODS

IRD analysis. Grain size studies and surface texture analysis conducted on the coarse component of non-biogenic sediments from high latitudes are widely used to identify IRD[5,8,11,15–17]. Samples were freeze-dried and gently broken apart using a pestle and mortar. Hydrogen peroxide was added to remove organic matter. Once diluted, 10% hydrochloric acid was added to remove carbonate. Following the method of ref. 30, biogenic silica was removed by adding 2M potassium hydroxide to the samples, placing them in a water bath at 85 °C, followed by an ultrasonic water bath set to 100% and 80 °C and centrifuged for 10 min at 3,000 r.p.m. The remaining residue was sieved at 63, 125, 250 μm and weighed. The MAR of IRD was calculated using the following equation:

IRD MAR = (%125 μm + %250 μm) × sedimentation rate × dry-bulk density

Grain size composition was visually determined using a stereo-binocular microscope.

Photographic techniques. Core photographs and dropstone images were taken using standard digital photography at the Bremen ODP Core Repository, Germany, and at the National Oceanography Centre, Southampton (NOCS), UK. Digital scanning electron micrographs were made using secondary electron imagery with a LEO 1450 VP scanning electron microscope at NOCS. Individual grains were picked, mounted on glue pads on aluminium pin stubs and sputter-coated with gold to a thickness of ~20 nm. Secondary electron images were obtained using operating conditions of 15 kV, a nominal probe current of 120 pA and a working distance of 14 mm.

Rock magnetic techniques. Rock magnetic parameters were measured for ~100 samples at NOCS. Standard 7 cm^3 samples were given an anhysteretic remanent magnetization in a dc field comparable to the Earth's magnetic field (50 μT). The samples were then subjected to stepwise alternating field demagnetization at 10 mT increments, to a maximum peak field of 30 mT, and measured in a cryogenic magnetometer inside a magnetically shielded laboratory. All samples were given an IRM in a pulse magnetizer, with an inducing field of 1.2 T. The $IRM_{1.2\,T}$ was then demagnetized with a backfield of 300 mT. Magnetic susceptibility was measured using a Bartington Instruments MS2B dual-frequency magnetic susceptibility meter. All magnetic parameters used in this study are listed in the Supplementary Information. The *S*-ratio was calculated as follows:

$$S\text{-ratio} = -IRM_{-0.3\,T}/IRM_{1.2\,T}$$

$$\text{'Hard' IRM} = (IRM_{1.2\,T} - IRM_{-0.3\,T})/2$$

Geochemical techniques. Additional data were generated from discrete samples (5 to 10 g of dried sediment), determined using X-ray fluorescence spectroscopy on a Xepos sequential X-ray spectrometer system at Ichron Ltd, UK.

Received 18 August 2006; accepted 8 January 2007.
Published online 7 February 2007.

1. Zachos, J. C., Pagani, M., Sloan, L., Thomas, E. & Billups, K. Trends, rhythms, and aberrations in global climate 65 Ma to present. *Science* **292,** 686–693 (2001).
2. Lear, C. H., Elderfield, H. & Wilson, P. A. Cenozoic deep-sea temperatures and global ice volumes from Mg/Ca in benthic foraminiferal calcite. *Science* **287,** 269–272 (2000).
3. Coxall, H. K., Wilson, P. A., Pälike, H., Lear, C. H. & Backman, J. Rapid stepwise onset of Antarctic glaciation and deeper calcite compensation in the Pacific Ocean. *Nature* **433,** 53–57 (2005).
4. Pekar, S. E., Hucks, A., Fuller, M. & Li, S. Glacioeustatic changes in early and middle Eocene (51–42 Ma): shallow-water stratigraphy from ODP Leg 189 Site 1171 (South Tasman Rise) and deep-sea $\delta^{18}O$ records. *Bull. Geol. Soc. Am.* **117,** 1081–1093 (2005).
5. Strand, K., Passchier, S. & Näsi, J. Implications of quartz grain microtextures for onset of Eocene/Oligocene glaciation in Prydz Bay, ODP Site 1166, Antarctica. *Palaeogeogr. Palaeoclimatol. Palaeoecol.* **198,** 101–111 (2003).
6. DeConto, R. M. & Pollard, D. Rapid Cenozoic glaciation of Antarctica induced by declining atmospheric CO_2. *Nature* **421,** 245–249 (2003).
7. Tripati, A., Backman, J., Elderfield, H. & Ferretti, P. Eocene bipolar glaciation associated with global carbon cycle changes. *Nature* **436,** 341–346 (2005).
8. Wolf-Welling, T. C. W., Cremer, M., O'Connell, S., Winkler, A. & Thiede, J. Cenozoic Arctic gateway paleoclimate variability: indications from changes in coarse-fraction composition (ODP Leg 151). In *Proc. ODP Sci. Res.* (eds Thiede, J., Myhre, A.M. & Firth, J.V.), **151,** 515–567 (ODP, College Station, Texas, 1996).
9. Moran, K. *et al.* The Cenozoic palaeoenvironment of the Arctic Ocean. *Nature* **441,** 601–605 (2006).
10. Winkler, A., Wolf-Welling, T. C. W., Stattegger, K. & Thiede, J. Clay mineral sedimentation in high northern latitude deep-sea basins since the Middle Miocene (ODP Leg 151, NAAG). *Int. J. Earth Sci.* **91,** 133–148 (2002).
11. Helland, P. E. & Holmes, M. A. Surface textural analysis of quartz sand grains from ODP Site 918 off the southeast coast of Greenland suggests glaciation of southern Greenland at 11 Ma. *Palaeogeogr. Palaeoclimatol. Palaeoecol.* **135,** 109–121 (1997).
12. Miller, K. G., Wright, J. D. & Fairbanks, R. G. Unlocking the icehouse: Oligocene-Miocene oxygen isotopes, eustasy, and margin erosion. *J. Geophys. Res.* **96,** 6829–6849 (1991).
13. Eldrett, J. S., Harding, I. C., Firth, J. V. & Roberts, A. P. Magnetostratigraphic calibration of Eocene-Oligocene dinoflagellate cyst biostratigraphy from the Norwegian-Greenland Sea. *Mar. Geol.* **204,** 91–127 (2004).
14. Myhre, A. M. *et al.* Site 913. *Proc. ODP Init. Rep.* **151,** 345–382 (1995).
15. Krinsley, D. H. & Doornkamp, J. C. *Atlas of Quartz Sand Surface Textures* (Cambridge Univ. Press, Cambridge, UK, 1973).
16. Clark, D. L. & Hanson, A. in *Glacial-Marine Sedimentation* (ed. Molnia, B. F.) 301–330 (Plenum, New York, 1983).
17. Nürnberg, D. *et al.* Sediments in Arctic ice: implications for entrainment, transport and release. *Mar. Geol.* **119,** 185–214 (1994).
18. Margolis, S. V. & Kennett, J. P. Cenozoic paleoglacial history of Antarctica recorded in subantarctic deep-sea cores. *Am. J. Sci.* **271,** 1–36 (1971).
19. Bond, G. *et al.* Evidence for massive discharges of icebergs into the North Atlantic ocean during the last glacial period. *Nature* **360,** 245–249 (1992).
20. Richter, T. O., Lassen, S., van Weering, T. C. E. & de Haas, H. Magnetic susceptibility patterns and provenance of ice-rafted material at Feni Drift, Rockall Trough: implications for the history of the British-Irish ice sheet. *Mar. Geol.* **173,** 37–54 (2001).
21. Karlin, R. & Levi, S. Diagenesis of magnetic minerals in recent hemipelagic sediments. *Nature* **303,** 327–330 (1983).
22. Hinrichs, J., Schnetger, B., Schale, H. & Brumsack, H.-J. A high resolution study of NE Atlantic sediments at station Bengal: geochemistry and early diagenesis of Heinrich layers. *Mar. Geol.* **177,** 72–92 (2001).
23. Upton, B. G. J., Emeleus, C. H. & Beckinsale, R. D. Petrology of the Northern East Greenland Tertiary flood basalts: evidence from Hold with Hope and Wollaston Forland. *J. Petrol.* **25,** 151–184 (1984).
24. Firth, J. V. Upper middle Eocene to Oligocene dinoflagellate biostratigraphy and assemblage variations in Hole 913B, Greenland Sea. *Proc. ODP Sci. Res.* **151,** 203–242 (1996).
25. Larsen, M., Heilmann-Clausen, C., Piasecki, S. & Stemmerik, L. in *Petroleum Geology: North-West Europe and global perspectives—Proceedings of the 6th Petroleum Geology Conference* (eds Doré, A. G. & Vinning, B. A.) 923–932 (The Geological Society, London, 2004).
26. Soper, N. J., Higgins, A. C., Downie, C., Matthews, D. W. & Brown, P. E. Late Cretaceous-early Tertiary stratigraphy of the Kangerdlugssuaq area, east Greenland, and the age of the opening of the north-east Atlantic. *J. Geol. Soc. Lond.* **132,** 85–104 (1976).
27. Harland, W. B. in *The Geology of Svalbard* (ed. Harland, W. B.) *Geol. Soc. Mem.* **17,** 363–387 (The Geological Society Publishing House, Bath, UK, 1997).
28. Deconto, R. M. & Pollard, D. Rethinking the Cenozoic record of ice volume: a modeling perspective on the relative contributions of Southern and Northern Hemispheres. *AGU Fall Meet. 2005* [CD] abstr. #PP52B–01 (American Geophysical Union, 2005); ⟨http://www.agu.org/⟩.
29. Pagani, M., Zachos, J. C., Freeman, K. H., Tipple, B. & Bohaty, S. Marked decline in atmospheric carbon dioxide concentrations during the Paleogene. *Science* **309,** 600–602 (2005).
30. Lyle, A. O. & Lyle, M. Determination of biogenic opal in pelagic marine sediments: a simple method revisited. *Proc. ODP Init. Rep.* **199,** 1–21 (2002).

Supplementary Information is linked to the online version of the paper at www.nature.com/nature.

Acknowledgements This research used samples provided by the Ocean Drilling Program (ODP). ODP was sponsored by the US National Science Foundation (NSF) and participating countries under management of the Joint Oceanographic Institutions (JOI, Inc.). We thank W. Hale and J. Firth for assistance with core examination and photography; S. Akbari, M. Houston and R. Helsby for sample preparation, Ichron for use of their XRF machine, B. Marsh for specimen photography and K. Davis for drafting the map.

Author Information Reprints and permissions information is available at www.nature.com/reprints. The authors declare no competing financial interests. Correspondence and requests for materials should be addressed to I.C.H. (ich@noc.soton.ac.uk).